

# 12 GHz CMOS MEMS Lab-on-chip System for Detection of Concentration of Suspended Particles in Bio-suspensions

Subhajit Guha, Alexander Wolf, Marco Lisker, Andreas Trusch,  
Chafik Meliani and Christian Wenger

*IHP, Leibniz Institute of Innovative Microelectronics, Im Technologie Park 25, Frankfurt(Oder), Germany*

**Keywords:** CMOS/MEMS, Lab-on-chip, Biosensor, High Frequency Bio-Sensor, CMOS Biosensor.

**Abstract:** This work presents a high frequency (X-band) CMOS dielectric sensor with hybrid microfluidic integration, applied to biosensing techniques; primarily to detect concentration of suspended particles in a solution. The detection technique is based on capacitive sensing of varying permittivity of the aqueous solution caused by different concentrations of suspended particles. The sensor chip is fabricated in 0.25  $\mu\text{m}$  SiGe:C BiCMOS technology of IHP with post processed PDMS microfluidic hybrid integration. The operating frequency of the sensor is 12.3 GHz and draws a DC power of approximately 35 mW from 3 V power supply. The dielectric sensitivity of the chip was characterized and calibrated using different organic fluids (alcohols); a sensitivity of 100 MHz/permittivity was measured with the sensor. After the calibration phase, the sensor was further used to measure the concentration of glucose in a homogeneous glucose solution. Frequency down-shift of 250 MHz/10% increase in water concentration in the homogeneous solution was observed. In order to analyse the concentration of suspended particles in a solution various concentrations of micro-beads in acetone solution were measured. Approximately a frequency up-shift of 125 MHz/10  $\mu\text{l}$  increase in bead volume in acetone was observed. The overall chip size is 2.76 mm<sup>2</sup>.

## 1 INTRODUCTION

Miniaturized sensors applied to biological and diagnostic purposes have led to approaches where measurement and analysis of extremely small volumes of assays are feasible. With the advent of micro-fabrication technique and its extension to microfluidic technology, analysis of samples in the order of few pico litres has become a reality. Such complex systems are termed as lab-on-chip (LOC) devices due to high level of miniaturization and also parallel analysis capabilities, analogous to a state of the art biotechnology laboratory. However, detection and sensing technique in such established LOC devices rely mainly on optical measurement techniques as explained by Pires et al (2014). Although optical measurements often provide a more visually precise result, the measurement systems are governed by bulky optical devices and test-benches. Therefore, the advantages of developing miniaturized LOC devices are no longer rational. Added to this, optical measurement techniques require bio-markers, referred as fluorescent markers and these markers can

additionally alter the properties of the assays. Therefore, adapting to a label free sensing approach, based on “all electrical” technique is absolutely imperative.

Established electrical analysis methods of biological suspensions rely on static amperometric techniques or impedance measurements demonstrated by various research groups like, Goh and Ram (2010), Krommenhoek et al (2006), Faenza et al (2012) and Rassaei et al (2012). Usually impedance measurements are performed at frequency range of 100 KHz to a few MHz as described by Krommenhoek et al (2006). In this frequency range (“low frequency”) biological suspensions show dielectric dispersions based on the properties of suspended particles, for example cells. Therefore, measurement and sensing in this frequency regime are competent for detection of low frequency properties of suspended particles or cells (for e.g. in case of cells, membrane capacitance). However, in order to detect concentration of particles or cells in a suspension such dispersions can be highly cumbersome and can lead to falsified measurement data. Additionally, “low frequency” measurement techniques also bring in electrode polarization

mechanism at the electrode electrolyte (biological suspension) interface, leading to another dispersion mechanism called the “ $\alpha$  dielectric dispersion”, described by Faenza et al (2012). Also double layer capacitance at the electrode electrolyte interface influences the impedance measurement and requires thorough modelling in order to incorporate its effects on the measurements. Thus, at lower frequencies, irrelevant dispersion effects and surface electro-chemistry have a strong influence, often making measurement and especially detection of concentration of suspended particles in a solution extremely complex. On the other hand, amperometric techniques allow very precise measurement but suffer from real miniaturization issues as a bulky reference electrode is needed for maintaining solution potential, as can be seen in approaches like the one described by Rassaei et al (2012). High frequency (in the order of tens of GHz) sensors can offer a potential solution to evade the aforementioned problems. The compatibility of such sensors with standard CMOS or BiCMOS process technology would further reduce fabrication costs, making them highly lucrative for biosensing approaches.

The advances in RF engineering have led research groups to explore high frequency characterization of biological suspensions and biomaterials. Grenier et al (2013) have demonstrated the distinction of living and dead cells using dielectric spectroscopy from 1 GHz to 40 GHz with a passive interdigitated electrode sensor. Ferrier et al (2009) have also shown interferometric microwave sensors for detection of single cells. A coplanar waveguide approach to characterize yeast cells was exhibited by Yang et al (2010). However, most of the aforementioned characterizing sensors are primarily passive structures realized on PCBs, therefore, pressing an ever increasing demand for complete CMOS or BiCMOS sensor system. In previous works, for e.g. Guha et al (2013), Guha et al (2014), we have demonstrated C-band to X-band complete CMOS microwave sensors for dielectric characterization of glucose solutions, biomaterials and also imaging of biomaterials. In this work, we report a complete CMOS/microfluidic system for dielectric detection of suspended particles in biological suspensions in the frequency range of 12 GHz. Hybrid integration of the microfluidic system to the CMOS chip is performed as a post process step after the chip fabrication. Simultaneous electrical and optical measurements of suspended particles in a solution depict close correlation of both the measurement. The X-band sensor described

in this work aids in avoiding low frequency dispersion mechanisms described previously. Thus, concentration of suspended particles can be unambiguously detected using such a high frequency sensor approach.

The dielectric sensing is based on capacitive scaling of an interdigitated capacitor (IDC), embedded in a CMOS cross coupled oscillator, analogous to a voltage controlled oscillator as explained by Lee (1998). In this report, the IDC acts as the variable capacitor. The capacitive scaling results in shift of resonant frequency of the CMOS oscillator. Therefore, the change of capacitance caused by the permittivity variation of the IDC ambient is read out as the resonant frequency shift of the oscillator. The permittivity variation is caused by the dielectric properties of the solutions flowing within the microfluidic channel aligned on top of the sensor.

## 2 SENSOR SYSTEM DESIGN

The complete sensor system design includes a two-step process. The CMOS dielectric active sensor chip (CMOS oscillator with the embedded IDC) is fabricated in the standard 0.25  $\mu\text{m}$  SiGe:C BiCMOS technology of IHP. The microfluidic system is made from polydimethylsiloxane (PDMS) using soft lithography technique with SU8 master mold. The sensor chip is diced from the wafer and bonded to the microfluidic system using oxygen plasma bonding technique.

### 2.1 Sensor Design

A multi-fingered planar IDC is used as the sensor in this work. The sensing principle is based on the variation of fringing electric fields between the fingers of the IDC, due to the change of permittivity on top of it. Fig. 1 (a) shows the 3D structure of an IDC with material under test (MUT) placed on top of it. The 2D IDC geometry shown in Fig. 1(b) defines the spatial wavelength of the structure  $\lambda_{\text{spc}}$ , which is the distance between two successive fingers on the same electrode, also given as  $\lambda_{\text{spc}} = 2(w+s)$ . In this report, the length  $l$  of the finger is 50  $\mu\text{m}$ , width  $w$  is 10  $\mu\text{m}$  and the spacing  $s$  is 20  $\mu\text{m}$ . The 2D simulation of a unit cell of the IDC in Fig. 1(c) shows the electric field patterns between two adjacent fingers of the IDC penetrating into the MUT. The permittivity of the MUT influences the electric fields and also the capacitance of the IDC. The fringing field capacitance can be analysed based

on the quasi static approximation of Maxwell's equations. Such an approximation can be utilized when the spatial wavelength ( $\lambda_{spc}$ ) of the IDC is comparatively much smaller than the operating wavelength ( $\lambda_{em}$ ) of the same. The operating wavelength is the wavelength of the electromagnetic wave defined by the frequency ( $\omega=2\pi f$ ) of operation, 12.3 GHz in our work. Therefore, the spatial wavelength ( $\lambda_{spc}=60 \mu\text{m}$ ) is considerably smaller compared to the operating wavelength ( $\lambda_{em} = 2.5 \text{ cm}$ ), and hence, quasi static approximation of Maxwell's equation holds well. The intensity of the electric field decays exponentially along the z direction as shown with simulation results in Fig. 1(c). The penetration depth ( $P_d$ ) of the electric field is defined as the distance from the IDC surface along the z direction, where the strength of the electric field is 1/e times the maximum field strength. Thus such a sensor can be effectively used for near field sensing approaches.

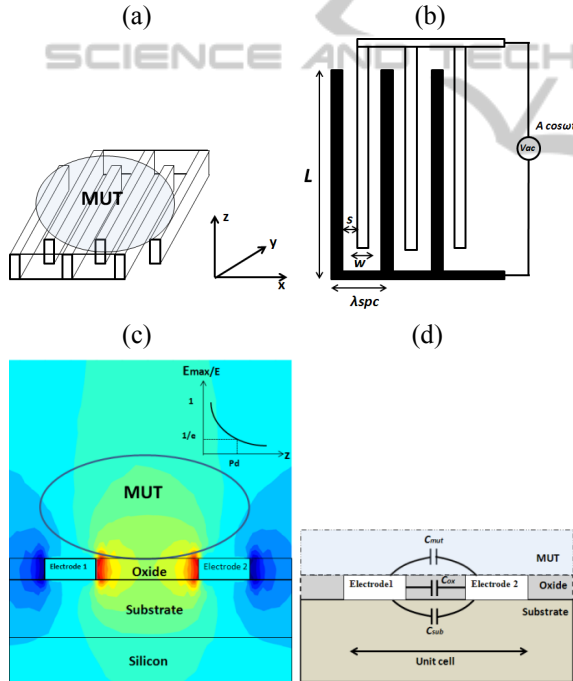


Figure 1: (a) 3D structure of IDC with MUT on top. (b) 2D geometry of the IDC. (c) 2D simulation of electric field in IDC (d) Modelling of IDC showing the different capacitive contributions.

The total per unit length capacitance of the unit cell of the IDC is the summation of the capacitive contributions due to the fringing fields penetrating into the substrate and the MUT and the parallel plate capacitive contribution due to the height of the fingers. The various capacitive contributions are

shown in Fig. 1 (d). The mathematical formulation of the capacitive contributions can be expressed as,

$$C_{unitcell} = C_{oxide} + C_{sub} + C_{MUT} \quad (1)$$

The fringing field capacitance per unit length due to the MUT and substrate is given by,

$$C_{sub} + C_{mut} = \epsilon_0 \left( \frac{\epsilon_{sub} + \epsilon_{mut}}{2} \right) \frac{K(\sqrt{1+k^2})}{K(k)} \quad (2)$$

where,  $K(k)$  is the solution of the infinite elliptical integral dependent on the geometry of the IDC. The total capacitance of the IDC is given as,

$$C_{IDC} = (N - 1)lC_{unitcell} \quad (3)$$

For a given geometry of the sensor, all the other capacitive contributions being effectively constant, the fringing field capacitance due to the MUT is the unique variable, depending on the permittivity of the MUT. The operating frequency of the sensor determines the frequency at which the electric fields within the MUT change their polarity. Thus, the permittivity of the MUT as sensed by the IDC is essentially the permittivity at the operating frequency.

In addition to the geometry, another very significant parameter of the sensor structure designed for high-frequency sensing technique is the self-resonating frequency (SRF) of the structure. SRF of a structure is defined as the frequency at which the capacitive contribution of the structure is nullified by its self-inductive contribution and the structure is purely resistive. The self-resonating phenomenon is shown in Fig. 2(a), where the resonance peak in the capacitance vs. frequency curve defines the frequency at which the IDC's self-inductance nullifies the capacitive contribution. The SRF is dependent on the size of the sensor and also on the permittivity of the substrate and the MUT. For a given geometry of the IDC on a specific substrate, the SRF is only dependent on the permittivity of the MUT. With the increase of the permittivity of the MUT the capacitance of the IDC increases and the SRF reduces as shown in Fig. 2(a). It is significant to design the operating frequency of the sensor system considerably lower than the SRF of the IDC. Fulfilment of such a condition ensures that the electric field in the IDC is rotation free and the structure is essentially capacitive. The simulated SRF of the IDC structure used in this work is beyond 150 GHz and the operating frequency of the oscillator circuit is 12 GHz. Thus, the structure is purely capacitive in the operating frequency range and Maxwell's equation in quasi static approximation can be applied, as discussed

previously. Equation 2 shows that the capacitance of the IDC increases with increase in the permittivity of the MUT, and the same is shown in the simulation results in Fig. 2(b) for the operating frequency around 12.3 GHz range. With respect to the sensing mechanism this up-shift of capacitance would be read out as a downscale of the resonant frequency of the oscillator.

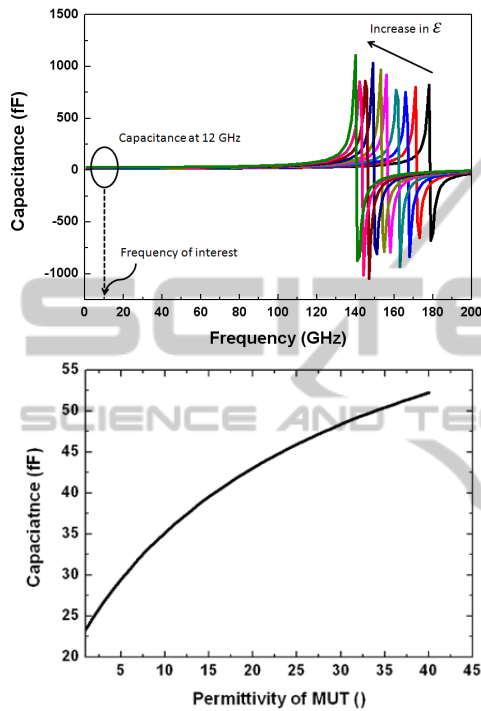


Figure 2: (a) Impedance simulation of IDC showing constant capacitance at desired frequency. The self-resonating frequency is far from the operating frequency. (b) Variation of capacitance of IDC with permittivity of MUT.

### 2.1.1 Fabrication of IDC

The IDC structure along with the CMOS oscillator is fabricated in the BiCMOS process line of IHP. Fig. 3(a) shows the planarised 0.25 μm SiGe:C BiCMOS back end of line (BEOL) stack with four metal layers. The bottom metal layers are lossy due to relatively small thickness as compared to the two top metal layers termed as TM1 and TM2. The IDC is designed in the lower loss TM2 metal layer of the BiCMOS stack. One major implication of the choice of the metal layer for designing the IDC, along with the influence on its quality factor is the influence of passivation layer. Passivation layer in micro-fabrication or CMOS technology is an insulation layer grown on top of the metal layers (electrodes) to protect the metal layers from external environment.

The passivation layer for a standard BiCMOS process is 400 nm of Si<sub>3</sub>N<sub>4</sub> (silicon nitride). In this work, in order to bond the PDMS microfluidic channel without further fabrication assisted steps, the standard Si<sub>3</sub>N<sub>4</sub> passivation layer is replaced by an SiO<sub>2</sub> (silicon dioxide) layer, followed by a Chemical Mechanical Polishing (CMP) planarization described by Lisker et al (2013). Therefore, when the IDC is designed on the topmost metal layer of the BiCMOS stack, as is done in this work, the passivation thickness is that of the height of SiO<sub>2</sub> and has a permittivity of 4.1.

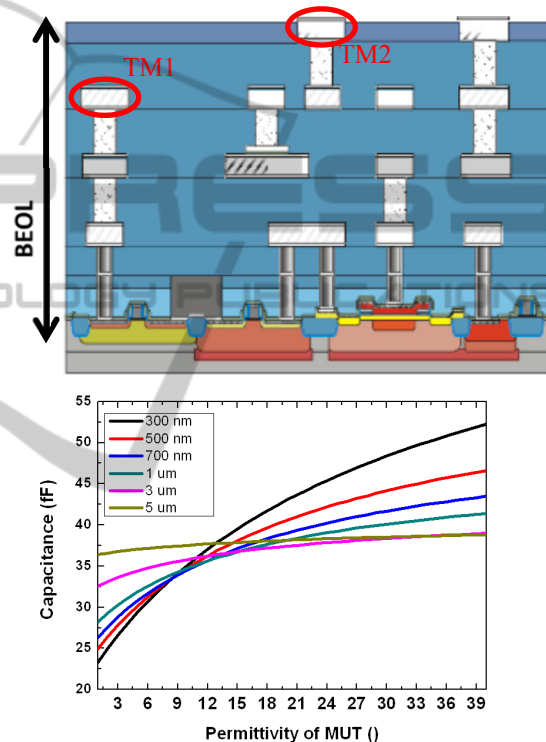


Figure 3: (a) Schematic cross section view of IHP's BiCMOS stack. The sensor is fabricated on the topmost metal layer of the stack. (b) Simulation of variation of capacitance with permittivity for different thicknesses of the SiO<sub>2</sub> layer.

The thickness and the permittivity of the SiO<sub>2</sub> layer influence the sensor sensitivity. If the IDC is designed on the TM1 layer of the BiCMOS stack, the SiO<sub>2</sub> layer has a thickness of approximately 5 μm. This is the combined height of SiO<sub>2</sub> on TM1 and SiO<sub>2</sub> on TM2. Fig. 3(b) shows the simulation of the influence of thickness of SiO<sub>2</sub> layer on the variation of capacitance due to permittivity change of MUT. The sensitivity of the stand-alone IDC is defined as the change of capacitance per unit change of permittivity, which is also given by the slope of the capacitance permittivity curve. The slope as

noted is reduced with the increase in the thickness of the SiO<sub>2</sub> layer as shown in Fig. 3b. Such a result is intuitive from the previous section, where the strength of the electric field was expected to decay exponentially along the z direction. The effect of SiO<sub>2</sub> is of wide interest for near field bio sensing, as often the electrodes are passivated to prevent them from coming in direct contact with the bio materials. It is shown with simulations that the sensor is sensitive up to a passivation thickness of 5 μm and thus can be efficiently used in near field bio sensing applications.

### 2.1.2 Sensor Circuit Design

The IDC is coupled with a pair of inductors to form an LC resonator. The inductor is also fabricated on the topmost metal layer of the BiCMOS stack (TM2). The simulated inductance of the inductor is 500 pH, and has a quality factor of approximately 15 at the operating frequency of 12 GHz. The resonant frequency of the oscillator is the function of the capacitance of the IDC. The schematic of the oscillator core with the sensor IDC and the inductors is shown in Fig. 4. A cross coupled pair of nMOS transistors drive the oscillation of the resonant LC oscillator. The resonant frequency of the oscillator core in the first order approximation is given as

$$f = 1/(2\pi\sqrt{2LC_{total}}) \quad (4)$$

where,  $L$  is the inductance of the individual inductor and  $C_{total}$  is the total capacitance of the IDC and the additional parasitic capacitances due to the transistors used in the active circuit. The total capacitance can be mathematically expressed as,

$$C_{total} = C_{IDC} + C_{parasitics} \quad (5)$$

The parasitic capacitances originate from the cross coupled transistors driving the oscillations of the LC resonator tank and also due to the transistors used in the buffer stage. The buffer stage isolates the oscillator core from subsequent stages of circuitry. The parasitic capacitance due to the transistors is dependent on the size of the transistors. For a transistor with a greater width of the channel ( $w_{channel}$ ), the parasitic capacitance is higher due to the area of the channel. On the other hand the channel width of the cross coupled nMOS transistors cannot be made sufficiently small, as wider transistors are required for sufficient transconductance ( $g_m$ ), to sustain the oscillation of the oscillator.

The total transconductance of the cross coupled transistors of the oscillator system nullifies the

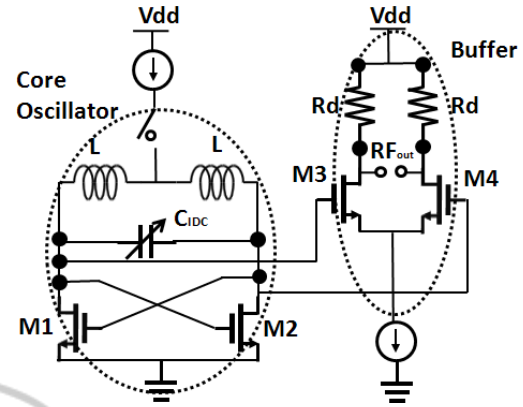


Figure 4: CMOS sensor circuit in cross coupled oscillator topology. The sensor IDC is used as the variable capacitor in the oscillator.

parasitic resistance of the inductor which would otherwise result in the damping and eventually dying of the oscillations.  $g_m$  is directly proportional to the width of the channel,  $w_{channel}$ . Hence there exists a trade-off between the channel width required for sufficient transconductance of the transistors and the parasitic capacitance due to the width of the channel. Parasitic capacitance reduces the sensitivity of the sensor system as they are in parallel to the sensor capacitance. For a given transistor size defined for the sufficient transconductance of the transistor, the parasitic capacitance is constant which is dependent only on the width of the transistor. The change of permittivity due to varied materials on top of the IDC, would change the  $C_{IDC}$  contribution of the total capacitance and in turn change the oscillating frequency of the oscillator. The sensitivity of the sensor which is the change of oscillating frequency with the change of permittivity on top of the IDC can be mathematically expressed as,

$$\frac{\delta f}{\delta \epsilon} = \frac{\delta f}{\delta C_{total}} \times \frac{\delta C_{total}}{\delta C_{IDC}} \times \frac{\delta C_{IDC}}{\delta \epsilon} \quad (6)$$

The output resistance  $R_d$  at the buffer stage is 50 ohms in order to match the resistance of the measuring probes. A standard DC power supply is used as the source for 3 V  $V_{dd}$  source as shown in the circuit schematic. A Rohde and Schwarz X-band spectrum analyser is used for measurement of the spectrum.

## 2.2 CMOS/Microfluidic Integration

PDMS (Polydimethylsiloxane) microfluidic channels of width 500 μm and height 50 μm was fabricated using SU8 master mold using soft lithography technique. The PDMS channel was

further bonded to the CMOS chip using oxygen plasma bonding technique. Fig. 5 shows the schematic view of the CMOS microfluidic system.

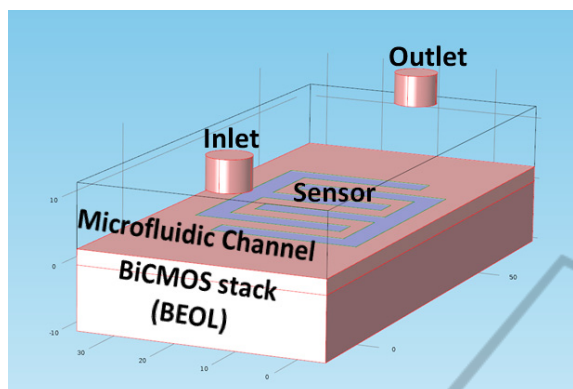


Figure 5: Schematic of hybrid CMOS/Microfluidic dielectric sensor system. The sensor is shown on top of the BiCMOS BEOL stack. The microfluidic channel is aligned on top of the sensor.

The BiCMOS wafer was polished using CMP (Chemical Mechanical planarization) technique to obtain a planar surface for precise bonding of the PDMS microfluidic system to the chip.

The master mold was fabricated from SU8 photoresist patterned on a 4 inch silicon wafer. SU8 is most commonly used for such fabrication techniques because of the capability of producing high aspect ratio structures with it. PDMS was prepared using Sylgard 184 Silicone elastomer base (Monomer) and its curing agent (hardener). The monomer and the hardener were mixed in the ratio 10:1. Other ratios of monomer to hardener were also tried for different elasticity of the PDMS structure. However, the above combination of monomer and hardener was chosen as it gave the best bonding strength. After thorough mixing, the solution was poured on the master mould and cured at a temperature of 70°C for ninety minutes. Room temperature curing is also possible but takes a longer time of approximately a day. The obtained PDMS structure was carefully peeled off from the mold and stored in a salinized chamber.

Oxygen plasma bonding of the PDMS microfluidic channel to the CMOS chip was performed in the Reactive Ion Etching (RIE) chamber. Plasma pressure of 16 Pa was used for a time of 30 seconds with an RF power of 65 Watt. Using higher RF power reduces the bonding strength as the PDMS surface which is changed from hydrophobic to hydrophilic due to the plasma action, to enable the bonding process, is transformed back to hydrophobic with higher RF power. Careful

alignment of the channel on top of the sensor was the limiting factor of the bonding time. The bonding time was kept within one minute in order to keep the PDMS in the activated state. Fig. 6 shows the process steps of the PDMS/CMOS hybrid microfluidic system.

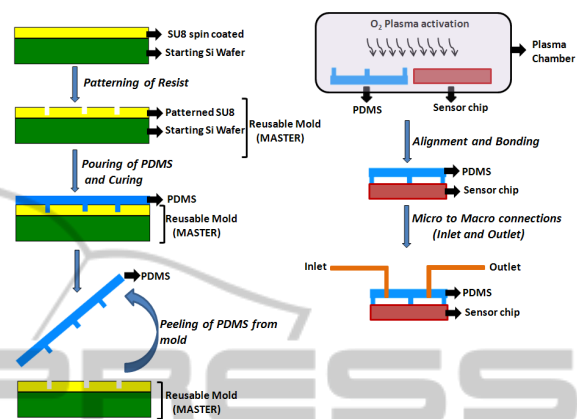


Figure 6: Fabrication steps of PDMS microfluidic channels and bonding to the silicon chip. The PDMS microfluidic channel is bonded to the silicon chip using oxygen plasma bond.

### 3 RESULTS AND DISCUSSION

The silicon chip bonded to the microfluidic system was measured in two steps. Initially microfluidic characterization of the chip was performed to check for leakage of the fluid. Leakage can often occur due to feeble bonding strength. Leakage of fluid from the microfluidic channel causes spreading of the fluid on the bond pads, thus, affecting the probes used for measurements or damaging the bond wires used for on board measurements. Therefore, once no leakage was confirmed, electrical measurements were performed on a wafer platform for stable measurements. Fig 7 shows the chip layout and the microfluidic tests after the hybrid integration of PDMS microfluidic channel. The channel is aligned on top of the sensor with the test fluid having no effect on the inductor coils.

The measurements were conducted in three steps. Calibration of the sensor was performed using organic fluids (Alcohols) of known permittivity in order to establish the sensitivity of the sensor and the detection limits.

Subsequently glucose solution was measured with varying concentration of water in the solution and finally concentration of suspended particles in acetone was measured. The measurement setup is shown in Fig. 8

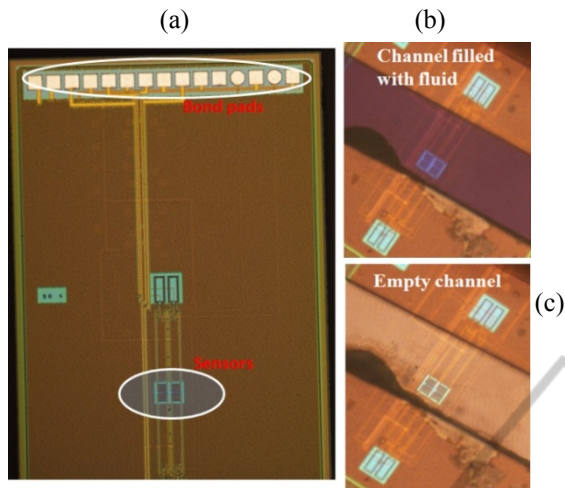


Figure 7: (a) Chip layout showing the sensors and the inductor coils. (b) Microfluidic channel with test fluid in it. The fluid flows only on top of sensor without influencing the inductors. (c) Empty microfluidic channel.

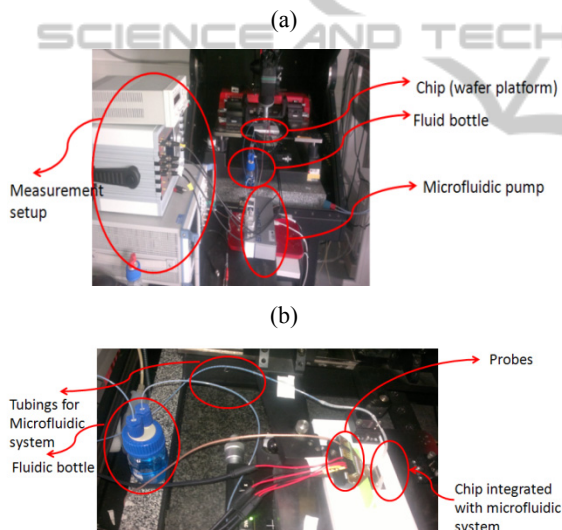


Figure 8: Measurement setup for the CMOS microfluidic system. The measurement is performed on the wafer station, shown in panel a. A DC power supply and a spectrum analyser is needed for measurement. Panel b shows the chip with the probes used for the measurement.

### 3.1 Calibration

The CMOS chips were characterized electrically prior to microfluidic experiments. The current drawn by the chip was 12 mA at an operating voltage of 3 V. The oscillating frequency was measured to be 12.32 GHz with an output power of -5 dBm. Further characterization of the chip was performed after plasma bonding of the PDMS microfluidic channel

with the chip. The DC operating values of the chip remained unaltered, while the oscillating frequency was measured to be 12.20 GHz. The 100 MHz shift of the oscillating frequency was accounted for the influence of the PDMS on the inductor coils used in the design of the oscillator. This resonant frequency served as the reference for further measurements, as the microfluidic channel was empty.

The variation of oscillating frequency of the dielectric sensor with materials of different permittivities was characterized by using organic fluids in the microfluidic system. A downshift of oscillating frequency was observed with increasing permittivity of the organic fluids, in this case alcohols. Fig. 9 shows the variation of the resonant frequency for different alcohols. At 12 GHz isopropanol and ethanol have almost the same permittivity ( $\epsilon = 3.8\sim 4.2$ ), as shown by Belrhiti et al (2012) and can be seen in the frequency output plot to be close to each other.

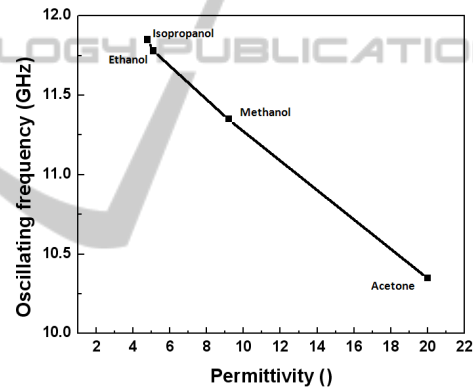


Figure 9: Calibration of sensor with organic fluids. Four different alcohols with different permittivities at 12 GHz were measured.

It is also noted that although the static permittivity of methanol is higher than the static permittivity of acetone, at 12 GHz, the permittivity of methanol is less than the permittivity of acetone described by Kung et al (1997) and the corresponding shift of resonant frequency shows the same.

Sensitivity of 100 MHz/permittivity was observed with the measurements performed with the organic alcohols. In order to estimate the measurement reproducibility microfluidic channels were bonded to five different sensor chips from the same wafer. Maximum frequency variation of 4 MHz was observed for same measurements and was negligible compared to the sensitivity of the sensor. The detection limit of the sensor can also be estimated with the measurement of isopropanol and

ethanol. The alcohols have a permittivity difference of 0.7 at 12 GHz and still show a considerable frequency shift as shown in Fig. 9.

### 3.2 Glucose Solution Measurement

The CMOS/microfluidic system was then used to study the effect of water in a homogeneous glucose solution. The variation of resonant frequency with different concentration of water depicts the variation of permittivity of the glucose solution with water content. Fig 10 shows the downshift of resonant frequency of the oscillator with increasing water content. Pure glucose solution has a permittivity of 8 at 12 GHz given by Meriakri et al (2006). The corresponding oscillating frequency is measured to be 11.52 GHz. This is close to the value measured for methanol ( $\epsilon = 9.2$ ) during calibration. The obtained results can be extended to determine permittivity of the glucose solution with different concentration of water.

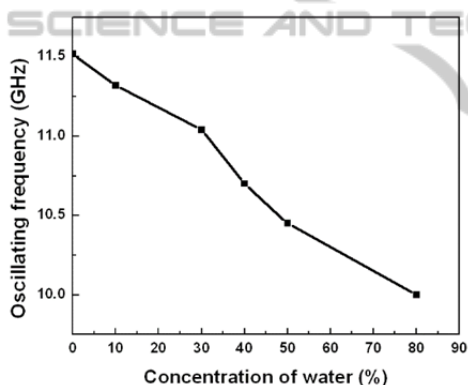


Figure 10: Measurement of water content in glucose solution using the dielectric sensor. The oscillating frequency down-shifts with increasing water content.

This can be related to the high permittivity of water at 12 GHz ( $\epsilon = 45$ ). With increasing water content the permittivity of the overall solution increases. The downshift of the oscillating frequency indicates an increase in permittivity with increasing concentration of water in the glucose solution. Every 10% increase in the water content shows a frequency down-shift of 250 MHz, which indicates a permittivity increase of approximately 2.5.

### 3.3 Micro-beads Measurement

Concentration of suspended particles in a bio suspension was emulated with micro-beads in acetone. Acetone was chosen as it showed the highest frequency shift during calibration of the

sensor. The influence of micro-beads or particles in a solution can be understood by the hindrance of molecular motion given by the Stokes-Einstein Debye equation described by Baisey-Fisher et al (2011). From the mathematical relation it can be understood that the characteristic Debye relaxation time increases or the characteristic frequency reduces with increasing concentration of particles in a suspension. In the higher GHz region where  $\gamma$  dispersion is predominant, the increase in particle concentration reduces the permittivity of the solution. In our measurement system we used micro-beads of diameter 10  $\mu\text{m}$  in different concentrations in a fixed volume of acetone 2 ml. The beads were thoroughly mixed in order to prepare a homogeneous solution.

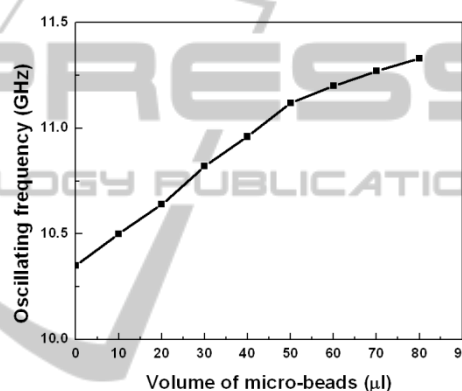


Figure 11: Measurement of micro-beads in acetone using the dielectric sensor. The oscillating frequency up-shifts with increasing concentration of beads.

Fig. 11 shows the variation of the oscillating frequency with increasing concentration of micro-beads. This is because the microfluidic channel is completely filled with the beads after a certain concentration of beads. This is shown in Fig. 12

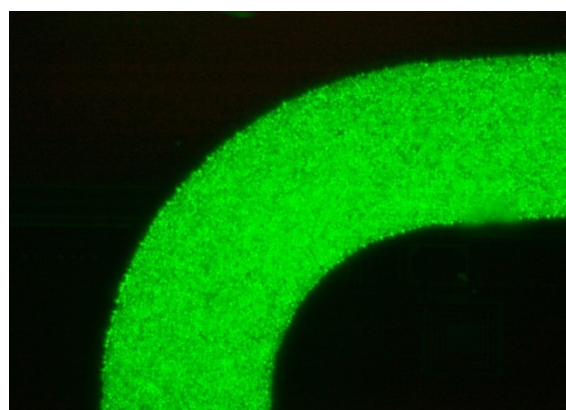


Figure 12: Fluorescent marked micro-beads showing the microfluidic channel being completely filled with the beads.

## 4 CONCLUSIONS

In this work a complete CMOS high frequency dielectric sensor with hybrid microfluidic integration was demonstrated. The operating frequency of the sensor is 12.3 GHz. A sensitivity of 100 MHz/permittivity was measured in the calibration phase performed with different organic liquids. Concentration of water in a homogeneous glucose solution was further measured using the sensor. 250 MHz/10% increase in water content in the glucose solution was observed. This could be further interpreted as an approximate increase of 2.5 in the permittivity of the solution. Concentration of suspended particles in a solution was further measured with micro-beads in acetone. Frequency up-shift of 125 MHz/10  $\mu$ l increase in bead content in acetone was measured. All in all a complete CMOS high frequency sensor with hybrid integrated microfluidic system was described. The advantages of using high frequency technique to detect concentration of particles in a suspension was investigated and demonstrated in this report.

## ACKNOWLEDGEMENTS

The authors would like to thank IHP technology department for the fabrication of the chip.

## REFERENCES

- Pires, N.M.M, Dong, T., Hanke, U., Hoivik, N. (2014) Recent Developments in Optical detection technologies in Lab-On-a-Chip Devices for Biosensing Application. *Sensors*.14. p. 15458-15479.
- Goh, S., and Ram, R.J. (2010) Impedance spectroscopy for in situ biomass measurements in microbioreactor. *14<sup>th</sup> International conference on Miniaturized Systems and Life Sciences*. Netherlands. p. 1556-1558.
- Krommenhoek, E.E., Gardeniers, J., Bomer, J., Van den Berg, A., Li, X., Ottens, M., van der Wielen, L., van Dedem, G., Van Leeuwen, M., van Gulik, W., Heijnen, J. (2006) Monitoring of yeast cell concentration using micromachined impedance sensor, *Sensors and Actuators*,B. 115.p. 384-389.
- Faenza, A., Bocchi, M., Pecorari, N., Franchi, E., Guerrieri, R.(2012) Impedance measurement technique for high sensitivity cell detection in microstructures with non-uniform conductivity distribution. *Lab Chip* 12(11). P.2046-2052.
- Rassaei, L., Goluch, E.D., Lemay, S. (2012). Substrate dependent kinetics in tyrosinase-based biosensing: Amperometry vs Spectrophotometry. *Analytical and Bioanalytical Chemistry*. 493. p.1577-1584.
- Grenier, K., Dubuc, D., Chen, T., Artis, F., Chretiennot, T., Poupot, M., and Fournié, J-J. (2013). Recent Advances in Microwave-based Dielectric Spectroscopy at the Cellular Level for Cancer Investigations *IEEE-TMTT* 61(4).p. 2023-2030.
- Ferrier, G.A., Romanuik, S.F., Thomson, D.J., Bridges, G.E., Freeman, M.R. (2009). A microwave interferometric system for simultaneous actuation and detection of single biological cells. *Lab on a Chip*. 9. p. 3406-3412.
- Yang, Y., Zhang, H., Zhu, J., Wang, G., Tzeng, T.-R., Xuan, X., Huang, K., Wang, P. (2010). Distinguishing the viability of a single yeast cell with an ultra-sensitive radio frequency sensor. *Lab on a Chip*. 10. p. 553-555.
- Guha, S., Jamal, F.I., Schmalz, K., Wenger, Ch., Meliani, Ch. (2013). CMOS lab on a chip device for dielectric characterization of cell suspensions based on a 6 GHz Oscillator. *European Microwave Conference*, Germany.
- Guha, S., Jamal, F.I., Schmalz, K., Wenger, Ch., Meliani, Ch. (2014) An 8 GHz CMOS Near Field Bio-sensor Array for Imaging Spatial Permittivity Distribution of Biomaterials. *IEEE MTT-S, Interantional Microwave Symposium*, USA.
- T.Lee (1998) *The design of CMOS Radio Frequency Integrated Circuits*,Cambridge.
- Lisker, M. Trusch, A., Fraschke, M., Kulse, P., Borokhovych, Y., Tillack, B., Ostermay, I., Krämer, T., Schmückle, F.-J., Krüger, O., Krozer, V., Heinrich, W. (2013). InP-Si BiCMOS Heterointegration Using a Substrate Transfer Process *ECS Transactions*. 53(245).
- Belrhiti, M.D., Bri, S., Nakheli, A., Haddad, M., Mamouni, A. (2012). Dielectric constant determination of liquid using rectangular waveguide structure combined with EM simulation. *J.Mater.Environ.Sci*. 3.p. 575-584.
- Kuang, W., Nelson, S.O. (1997). Dielectric relaxation characterization of fresh fruits and vegetables from 3 to 20 GHz. *J. of Microwave power and electromagnetic energy*. 32. p. 114-122.
- Meriakri, V V., Chigrai, E E., Kim, D., Nikitin, I.P., Pangonis, L.I., Parkhomenko, M.P., Won, J.H. (2006). Dielectric properties of glucose solutions in the millimetre-wave range and control of glucose content in blood. *IOP, Meas. Sci. Technology*. 18.p. 1-6.
- Basey-Fisher, T.H., Hanham, S.M., Maier,S.A., Stevens, M.M., Alford, N.M., Klein, N.( 2011).Microwave relaxation analysis of Dissolved Proteins:Towards free solution biosensing. *Applied Physics Letters* 99.